J. of Korean Meteor. Soc.
Vol. 30, No. 4, 1994

Implementation of Cloud-Topped Mixed Layer in a General Circulation Model

Jai-Ho Oh*, YiGn Noh, Jong-Jin Back, and Seung-Man Lee

Department of Astronomy and Atmospheric Sciences and Global Environment Laboratory, Yonsei University
134 Shinchon-dong, Seodaemun-ku, Seoul 120-749
(Manuscript received 9 June 1994)

대순환 모형에서 CTML 모형의 이용

오재호 · 노의근 · 백종진 · 이승만

연세대학교 천문대기과학과 지구환경연구소
(1994년 6월 9일 접수)

요 약

대규모 발산이 있으면서 상대적으로 해양이 차가운 지역의 해양성 행성경계층 구름을 재현하기 위해 꼭대기에 구름이 있는 혼합층 모형을 시험했다. Lilly(1968)의 모형을 기본으로 한 Guinn과 Schubert(1989)의 꼭대기에 구름이 있는 진단적 혼합층 모형(CTML)을 요약하고, 이 모형의 완성도를 평가하기 위해 일차원 민감도 실험을 수행했다. SST와 대규모 발산 그리고 지표 바람 속도의 다양한 조건에 따라 수행된 민감도 실험의 결과들을 살펴보므로써 구름의 뚜렷한 행태를 알 수 있었다. 그 결과들은 다음과 같다: 1) SST가 증가할 때, 구름의 꼭대기와 함께 밑바닥의 높이도 증가하지만 구름은 더욱 깊어지고 습해지며, 2) 대규모의 하층 발산이 약간 있으면 구름이 매우 깊어질 수도 있지만, 대규모의 하층 발산은 구름의 꼭대기와 밑바닥 양쪽에서 구름을 줄어들게 하고, 3) 바람 속도가 증가하면 지면의 현열과 수증기의 교환을 증가시켜 구름은 꼭대기와 밑바닥 양쪽에서 깊어지고, 상당 온위와 혼합층의 수증기 또한 증가하고, 4) 동태평양의 전형적인 종관 상태에서 해양성 구름은 연직으로 100 m-4,000 m 영역 안에 존재함을 보였다.

이 CTML 모형이 연세대학교의 대기대순환모형(YONU GCM)에 응용되었다. 두 달 간의 GCM 적분 실험을 통해 제시된 CTML 모형이 대규모 발산이 있고 해양이 차가운 무역풍 지역의 해양성 층적운을 잘 나타낼 수 있음을 보였다.

Abstract

A cloud-topped mixed layer model has been tested to represent the marine planetary boundary layer clouds over the region of large-scale divergence and relatively cool ocean surface. The Guinn and Schubert's (1989) diagnostic cloud-topped mixed layer (CTML) model, which is based on the Lilly's (1968) model, is summarized and tested in one-dimensional sensitivity experiments to evaluate the performance of this proposed CTML model. Based on the results of sensitivity tests under the various SSTs large-scale divergences and surface wind speed conditions we may observe a reasonable behavior of clouds. The results are; 1) as SST increases, the cloud becomes deeper and more moistened, although the cloud base also increases along with the cloud top, 2) the cloud can be very deep with a small large-scale low-level divergence, but the large-scale low-level

*현재 기상청, 기상연구소에 근무

divergence may shrink the cloud depth in both directions of the top and bottom, 3) the cloud becomes deeper by lowing the cloud bottom and elevating the cloud top, and the equivalent potential temperature and moisture of the mixed layer also increase as the wind speed increases due to the enhanced surface sensible heat and moisture exchanges, 4) under the typical synoptic situations in the eastern Pacific the proposed CTML model predicts the marine cloud depth of 100 m to 4,000 m.

This proposed cloud-topped mixed layer (CTML) model has been applied to the Yonsei University general circulation model (YONU GCM). Through a series of two months GCM integration experiments we observe the proposed diagnostic CTML model has a capability to improve notably the marine stratocumulus at the region where the large-scale mass diverges above the cool sea surface in the trade-wind zone.

1. Introduction

Recently, it has been recognized that the stratocumulus plays a very important role in the climate change (*e.g.*, Charlson *et al.*, 1987). However, the proper representation of the marine stratocumulus related to the large-scale mass divergence and the oceanic cool waters in the trade-wind zone is one of the most difficult tasks in the general circulation model (GCM) (Albrecht *et al.*, 1990), particularly in, the shallow cloud layer associated with marine stratocumulus.

There are many observational studies to understand the physical processes governing the formation, maintenance and dissipation (Randall *et al.*, 1984; Cox *et al.*, 1987; Albrecht *et al.*, 1988; Kloesel, 1992; Wang and Albrecht, 1992). Also, there are many modeling efforts to reproduce the low level marine clouds with the coupling of radiation and turbulence processes in the manner of mixed-layer approach (Lilly, 1968; Deardorff, 1976; Kraus and Schaller, 1978; Schubert *et al.*, 1979; Turton and Nicholls, 1987), turbulence closure approach (Chen and Cotton, 1987; Roger and Koracin, 1992), mixing line approach (Betts and Bores, 1990), and mass flux approach (Betts, 1973; Rogers *et al.*, 1985; Wang, 1993). Recently, Randall *et al.* (1992) used a combined method of turbulence closure and mass flux approaches.

The YONU GCM has employed the same cloud and radiation scheme as in the University of Illinois GCM (UILL GCM, formerly the Oregon State University multilayer GCM, Oh, 1989) which has successfully simulated the cloud climatology and the earth's radiative budget terms at the top of atmosphere compared to the satellite observations with a physically-based parameterization of cloud and radiative transfer scheme (Oh, 1989). However, the marine stratocumulus and stratus in the subtropical regions are significantly underestimated due to the lack of planetary boundary layer cloud scheme in the UILL GCM. To overcome this under-estimation of the subtropical stratus and stratocumulus the Guinn and Schubert's (1989; here after GS) diagnostic cloud-topped mixed model, which is based on the Lilly's (1968) model, is tested by coupling it with the YONU GCM in this study.

The Lilly's (1968) original cloud-topped mixed layer model and GS's steady-state, horizontally homogeneous, cloud-topped marine boundary layer model based on it are introduced in section 2 and 3, respectively. We have modified the Guinn and Schubert's model for the YONU GCM and discussed the results of this cloud-topped mixed layer model in section 4. Betts and Ridgway (1989, here after BR) also studied a similar equilibrium experiments with one dimensional boundary layer model over the tradewind region. For the qualitative evaluation of this experiment the works of BR have been compared. Finally the conclusions are made in section 5.

2. Lilly's Model

Lilly (1968) developed the cloud-topped mixed layer model based on the requirement that the wet-bulb potential temperature must increase in the inversion. In the Lilly's theory, the strong or moderate subsidence is heating the mixed layer while the radiation from the top of cloud would exert a cooling effect in the mixed layer. He disregarded the effects of the surface shear due to the length scale (introduced

by Monin and Oboukhov) of the shear-generated turbulence is much smaller than the thickness of the mixed layer which is 500 to 1,000 meters or more.

2.1. Dry Cloud-Topped Layer

For the simplified illustration of the mechanism, the dry cloud is considered. The surface turbulent heat flux is assumed in the form

$$(\overline{w'\theta'})_0 = C_T V_0 (\theta_S - \theta_0), \tag{1}$$

where w is the vertical velocity, θ is the potential temperature, C_T is the heat transfer coefficient, V_0 the surface wind, the subscript 0 represents the variables at a small height above the surface, and the subscript S represents the variables at the surface. If this flux is positive it is assumed that the entire mixed layer (from $z = 0$ to $z = H$) is filled with cloud.

Under the assumption that H is much smaller than the scale height of the atmosphere, the thermal equation for the cloud -topped mixed layer can be written as

$$\frac{\partial \theta_0}{\partial t} = -\frac{\partial}{\partial z}(\overline{w'\theta'}). \tag{2}$$

Since θ_0 is constant with height, by integrating Eq. (2) from surface to H,

$$\frac{\partial \theta_0}{\partial t} = \frac{1}{H}[(\overline{w'\theta'})_0 - (\overline{w'\theta'})_H]. \tag{3}$$

The heat balance equation at the top of cloud layer is

$$\left(\frac{\partial H}{\partial t} - w_H\right)(\theta_{UH} - \theta_0) + (\overline{w'\theta'})_H = F_{UH}, \tag{4}$$

where the subscripts H and UH refer, respectively, the properties of the cloud layer just below and above its top, and F is radiative cooling.

Based on Ball (1960) the turbulent energy equation, integrated over the mixed layer depth may be written as

$$\int_0^H \left(\frac{\partial E}{\partial t} + w\frac{\partial E}{\partial z}\right)dz = g\int_0^H \frac{\overline{w'\theta'}}{\overline{\theta}}dz - (\overline{w'E'})_H - \int_0^H \varepsilon dz, \tag{5}$$

where E is the turbulent kinetic energy (TKE), E' is the eddy turbulent kinetic energy, ε is the rate of molecular dissipation rate of the TKE, $\overline{w'E'}$, is a shorthand notation for the pressure-velocity and triple velocity product terms. The generation and the dissipation of shear-driven turbulence in the lowest levels have been ignored as mentioned above. Through the scale analysis (Lilly, 1968) the steady-state of Eq. (5) becomes

$$-g\int_0^H \frac{\overline{w'\theta'}}{\overline{\theta}}dz + (\overline{w'E'})_H + \int_0^H \varepsilon dz = 0. \tag{6}$$

The problem can be considered in two cases of the minimum and maximum entrainment as shown in Fig. 1, respectively. A detailed explanation is as follows:

Maximum entrainment

Ball (1960) hypothesized that the dissipation and the transport term of Eq. (6) are negligible compared to the positive and negative contributions by turbulent heat fluxes, so that

$$\int_0^H \overline{w'\theta'}dz = 0 \quad \text{but} \quad \overline{w'\theta'} \neq 0, \text{ some where.} \tag{7}$$

With the assumption of linearly varying heat-flux, the

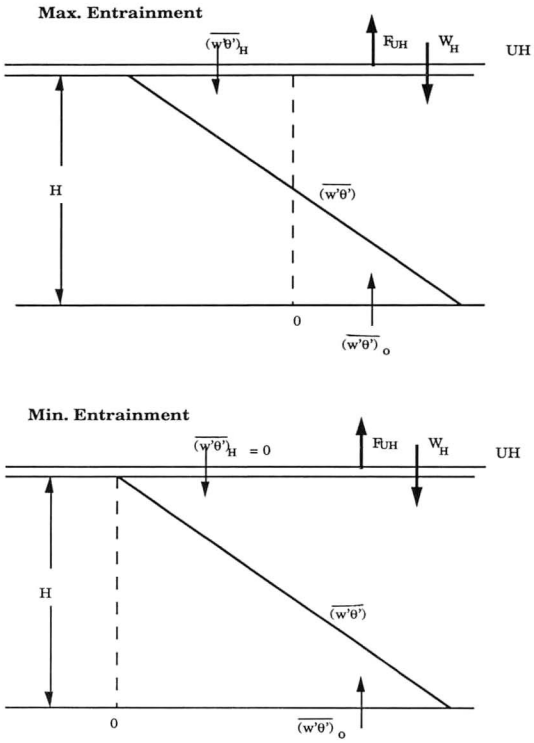

Fig. 1. Schematic diagram for the maximum and minimum entrainment of the dry mixed layer in the upper and lower panel, respectively. The symbols are illustrated in the text.

Ball's hypothesis leads to

$$(\overline{w'\theta'})_H = -(\overline{w'\theta'})_0, \\ = C_T V_0(\theta_S - \theta_0). \quad (8)$$

Combining Eqs. (8) and (1) with Eqs. (3) and (4) we obtain a close set of equations for the maximum entrainment case:

$$\frac{\partial \theta_0}{\partial t} = \frac{2}{H} C_T V_0(\theta_S - \theta_0), \quad (9)$$

and

$$\frac{\partial H}{\partial t} - w_H = \frac{F_{UH} + C_T V_0(\theta_S - \theta_0)}{\theta_{UH} - \theta_0}. \quad (10)$$

Minimum entrainment

The minimum possible entrainment is zero, but a more probable minimum of entrainment is set by Lilly (1968) as

$$(\overline{w'\theta'})_H = 0,$$
$$(\overline{w'\theta'})_{\text{min imum}} = 0 \text{ but } \int_0^H \overline{w'\theta'} dz > 0. \quad (11)$$

applying Eqs. (11) and (1) with Eqs. (3) and (4) we obtain a close set of equations for the minimum entrainment case:

$$\frac{\partial \theta_0}{\partial t} = \frac{1}{H} C_T V_0(\theta_S - \theta_0), \quad (12)$$

and

$$\frac{\partial H}{\partial t} - w_H = \frac{F_{UH}}{\theta_{UH} - \theta_0}. \quad (13)$$

2.2. Moist Cloud-Topped Layer

To simplify the thermodynamics for a mixed layer which is thin compared to the scale height of the atmosphere, Lilly (1968) constructed a linearized condensation model. The Clausius-Clapeyron equation combined with the hydrostatic equation can be written as (see Appendix A)

$$dq^* = ad\theta - bdz, \quad (14)$$

where

$$a = \frac{\delta L}{RT} \frac{q^*}{\theta}, \quad (15)$$

and

$$b = \frac{g}{RT} q^* \left(\frac{\delta L}{c_p T} - 1 \right) \quad (16)$$

with q^* the saturated mixing ratio of water vapor at the temperature T, δ the coefficient (= 0.622), L the latent heat of vaporization, R the gas constant, g the gravity, and c_p the specific heat at constant pressure.

Let's define the wet-bulb potential temperature, θ_w, as fundamentally a measure of the total sensible plus latent heat content of the air, specifically

$$(1+\alpha)d\theta_w = d\theta + \frac{L}{c_p} dq, \quad (17)$$

where $\alpha = aL / c_p$.

By combining Eqs. (16) and (17) we can show that the moist adiabatic lapse rate of q and q are given by

$$\left(\frac{\partial \theta}{\partial z}\right)_{\theta_w} = \frac{b}{a} \frac{\alpha}{1+\alpha}, \left(\frac{\partial q}{\partial z}\right)_{\theta_w} = -\frac{b}{1+\alpha} \quad (18)$$

and using Eqs. (14) and (18) we can write Eq. (17) in the form

$$d\theta_w = d\theta - \left(\frac{\partial \theta}{\partial z}\right)_{\theta_w} dz_c, \quad (19)$$

where z_c is the level of lifting condensation.

As a measure of relative buoyancy, the virtual potential temperature, θ_v, can be defined as

$$d\theta_v = d\theta + \overline{\theta}(\delta dq - dm), \quad (20)$$

where $\delta = 0.608$, $\overline{\theta}$ is a reference temperature and m is the liquid water content.

The above expression are valid both for mean and fluctuating quantities. Thus we can have

$$(1+\alpha)\overline{w'\theta'_w} = \overline{w'\theta'} + \frac{L}{c_p} \overline{w'q'}, \quad (21)$$

and

$$\overline{w'\theta'_v} = \overline{w'\theta'} + \overline{\theta}(\delta \overline{w'q'} - \overline{w'm'}). \quad (22)$$

The entrainment conditions, which are necessary to close the system, are chosen in exact analogy with the dry case except for the use of the virtual temperature flux. These are

$$\text{Maximum: } \int_0^H \overline{w'\theta'_v} dz = 0 \\ \text{but } \overline{w'\theta'_v} \neq 0 \text{ somewhere.} \quad (23)$$

$$\text{Minimum: } (\overline{w'\theta_v'})_{\text{minimum}} = 0 \text{ but } \int_0^H \overline{w'\theta_v'}dz > 0. \tag{24}$$

The flux term $\overline{w'\theta_v'}$ can be expressed in terms of the conserving variables during the change of phase of water by Eqs. (21) and (22) as

$$\overline{w'\theta_v'} = (1+\alpha)\overline{w'\theta_w'} - \bar{\theta}\overline{w'(q'+m')} - \left[\frac{L}{c_p} - \bar{\theta}(\delta+1)\right]\overline{w'q'}. \tag{25}$$

Using Eqs. (14) and (19) to show that $\overline{w'q'} = a\overline{w'\theta_w'}$ at the constant height for the cloud layer, we can rewrite Eq. (25) in the form

$$\overline{w'\theta_v'} = \begin{cases} (1+\alpha)\overline{w'\theta_w'} - \left(\dfrac{L}{c_p} - \bar{\theta}\delta\right)\overline{w'q'}, & \text{for } z < h \\ [1+a\bar{\theta}(\delta+1)\overline{w'\theta_w'} - \bar{\theta}\overline{w'(q'+m')}, & \text{for } z \geq h \end{cases} \tag{26}$$

which can be evaluated in terms of boundary quantities since each of the component flux terms has a linear form.

The maximum entrainment condition can be obtained by carrying out integration of Eq. (23) in the form

$$\begin{aligned} &\left(1+\alpha_1\frac{h^2}{H^2}\right)(\overline{w'\theta_w'})_H \\ &-\frac{1}{a}\left(\beta_1+\alpha_1\frac{h^2}{H^2}\right)\overline{w'(q'+m')_H} \\ &= -\left[1+\alpha_1\frac{h}{H}\left(2-\frac{h}{H}\right)\right]\overline{(w'\theta_w')_0} \\ &+\frac{1}{a}\left[\beta_1+\alpha_1\frac{h}{H}\left(2-\frac{h}{H}\right)\right]\overline{(w'q')_0} \end{aligned} \tag{27}$$

with

$$\alpha_1 = \frac{\alpha - a\bar{\theta}(\delta+1)}{1+a\bar{\theta}(\delta+1)}, \quad \beta_1 = \frac{a\bar{\theta}}{1+a\bar{\theta}(\delta+1)}. \tag{28}$$

The minimum entrainment condition is

$$\text{Minimum}\left\{\begin{array}{l} (1+\alpha)\overline{w'\theta_w'} - \left(\dfrac{L}{c_p} - \bar{\theta}\delta\right)\overline{w'q'}, \\ \text{for } z < h \\ [1+a\bar{\theta}(\delta+1)]\overline{w'\theta_w'} - \bar{\theta}\overline{w'(q'+m')}, \\ \text{for } z \geq h \end{array}\right\} = 0. \tag{29}$$

The cloud base level h is evaluated by integrating Eq. (14) as

$$\begin{aligned} h &= \frac{1}{b}[q_S - q_0 - a(\theta_S - \theta_0)] \\ &= \frac{1}{b}(1+\alpha)[q_S - q_0 - a(\theta_{wS} - \theta_{w0})] \\ &= \frac{1}{b}(q_0{}^* - q_0). \end{aligned} \tag{30}$$

3. Guinn and Schubert's Steady-State Model

GS developed a steady-state, horizontally homogeneous, cloud-topped marine boundary layer model based on the work of Lilly (1968). The differences from the Lilly's (1968) model are:

(1) radiation is allowed to penetrate into the boundary layer;

(2) the closure assumption assumes a weighted average of Lilly's (1968) maximum and minimum entrainment cases.

(3) cloud top values of longwave radiation, equivalent potential temperature and water vapor mixing ratio are linearly specified based on the observational data.

3.1 Radiation Parameterization

Schubert *et al.* (1979) allowed the radiative cooling through the mixed layer, such that the changes in radiative fluxes across cloud top and at the mixed layer as

$$F_U - F_H = (\rho c_p)^{-1}[(1-\mu)(\sigma T_H^4 - R_U^{\downarrow}) - (1-\mu')S], \tag{31}$$

and

$$F_H - F_S = (\rho c_p)^{-1}[\mu(\sigma T_H^4 - R_U^{\downarrow}) - \mu' S], \tag{32}$$

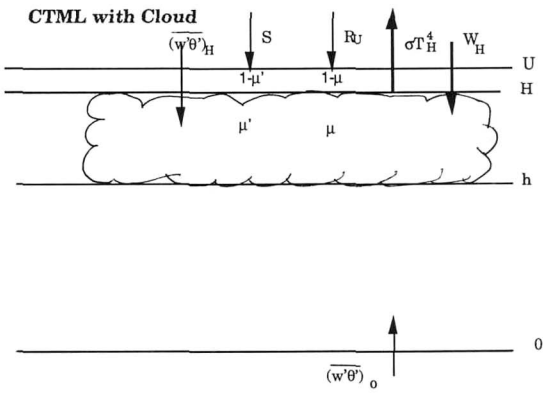

Fig. 2. Schematic structure of fluxes in the cloud-topped mixed layer. The symbols are illustrated in the text.

where ρ is the constant air density, σ is the Stefan-Boltzmann constant, T_H is the cloud top temperature, $R_U^{\downarrow}$ is the downward longwave radiative flux above the mixed layer, S is the absorbed solar radiation, and μ and μ' are the longwave and shortwave partitions, respectively. Figure 2 shows a schematic structure of fluxes in this cloud-topped mixed layer.

The absorbed solar radiation is assumed to be S = 22.3 Wm^{-2} as suggested by Lilly (1968). The downward longwave radiative flux above the mixed layer is formulated based on the climatological data in the form

$$R_U^{\downarrow} = \begin{cases} 314.0 + 0.03077H, & \text{for Oakland} \\ 333.1 + 0.32360H, & \text{for San Diago} \end{cases} \tag{33}$$

The cloud top temperature is calculated as follows: Using Eq. (18) we obtain the potential temperature at the top of mixed layer as

$$\theta_H = \theta_h + \frac{b}{a}\left(\frac{\alpha}{1+\alpha}\right)(H-h), \tag{34}$$

where the potential temperature at the base of cloud, θ_h, can be calculated from the conservative thermodynamic variables and the definition of equivalent potential temperature, i.e.,

$$\theta_h = \theta_e - \frac{L}{c_p}(q+m). \tag{35}$$

In Eq. (35) θ_e is the equivalent potential temperature of mixed layer. Then the cloud top temperature can be calculated as

$$T_H = \left[\theta_h + \frac{b}{a}\left(\frac{\alpha}{1+\alpha}\right)(H-h)\right]\left(\frac{p_H}{p_0}\right)^{\frac{R}{c_p}} \tag{36}$$

3.2 The Combined Convective-Radiative Model

The basic equations and assumptions for the moist cloud-topped model with radiative processes can be written as follows: The mixed layer budget equations for the equivalent potential temperature and moisture are

$$\frac{\partial \theta_e}{\partial t} = \frac{1}{H}[\overline{(w'\theta_e')_0} - \overline{(w'\theta_e')_H} - (F_H - F_S)] \tag{37}$$

and

$$\frac{\partial q_0}{\partial t} = \frac{1}{H}[\overline{(w'q')_0} - \overline{w'(q'+m')_H}]. \tag{38}$$

The equation (37) is the same as Eq. (3), except for the equivalent potential temperature and the additional radiative flux term in the r.h.s. which represents the change in radiative flux across the mixed layer. The equivalent potential temperature and total water in the mixed layer are assumed as

$$\theta_e = \theta_{0e}, \text{ and } q+m = q_0. \tag{39}$$

The surface fluxes are assumed in the form

$$\overline{(w'\theta_e')_0} = C_T V_0(\theta_{eS} - \theta_e) \tag{40}$$

and

$$\overline{(w'q')_0} = C_T V_0(q_S - q_0). \tag{41}$$

The equivalent potential temperature at the top of cloud can be written as

$$\left(\frac{\partial H}{\partial t} - w_H\right)(\theta_{eU} - \theta_e) + \overline{(w'\theta_e')_H} = F_U - F_H. \tag{42}$$

The jumps of the equivalent potential temperature and total water across the top of cloud can be written as

$$\Delta\theta_e = \theta_{eU} - \theta_e, \text{ and } \Delta(q+m) = q_U - (q+m). \tag{43}$$

Eq. (42) can be written as

$$\frac{\partial H}{\partial t} = \frac{1}{\Delta\theta_e}[F_U - F_H - \overline{(w'\theta_e')_H}] - DH. \tag{44}$$

Here w_H is expressed as w_H = -DH where D is the large scale divergence. The cloud base level h can be

obtained from Eq. (30) as

$$h=\frac{1}{b}[(1+\alpha)(q_S-q_0)-a(\theta_{eS}-\theta_{e0})], \tag{45}$$

if we assume that

$$d\theta_e \cong (1+\alpha)d\theta_w \tag{46}$$

over a shallow height interval compared to the atmospheric scale height as in the case of Lilly (1968). For the consistency and the closure assumption the relation between the potential temperature entrainment and moisture entrainment can be written with a simple matrix notation form as

$$\begin{bmatrix} a_{11} & a_{12} \\ a_{21} & a_{22} \end{bmatrix} \begin{bmatrix} \overline{(w'\theta_e')_H} \\ \overline{\theta w'(q'+m')_H} \end{bmatrix} = \begin{bmatrix} b_1 \\ b_2 \end{bmatrix}, \tag{47,48}$$

where a_{ij} and b_i are coefficients. Now, we have twelve unknowns H, h, θ_e, q_0, $\Delta\theta_e$, T_H, $(F_U - F_H)$, $(F_H - F_S)$, $\overline{(w'\theta_e')_0}$, $\overline{w'(q'+m')_0}$, $\overline{(w'\theta_e')_H}$, and $\overline{w'(q'+m')_H}$ and the twelve equations (31), (32), (36) - (38), (40), (41), (43) - (45), (47) and (48).

3.3 The Steady-State Solutions

By reducing the above set of equations to one equation of H in the steady state we can iteratively get the steady-state solution as follows; the surface fluxes of equivalent potential temperature and moisture are expressed by eliminating the dependent variables θ_e and $\overline{(w'\theta_e')_H}$ in Eqs. (37), (40), and (44). The resulting expression is

$$\overline{(w'\theta_e')_0}=\frac{(F_U-F_H)+(F_H-F_S)+DH(\theta_{eS}-\theta_{eU})}{\left(1+\frac{DH}{C_TV_0}\right)} \tag{49}$$

Similarly, from Eqs. (38), (39), (41), and (43) we obtain

$$\overline{w'(q'+m')}=\frac{DH(q_S-q_U)}{\left(1+\frac{DH}{C_TV_0}\right)}. \tag{50}$$

Note that the total water flux is constant with height in the steady-state solution. Also, we can eliminate θ_e and q_0 in Eq. (45). The resulting cloud base height expression is

$$h=\frac{(1+\alpha)\overline{w'(q'+m')}-a\overline{(w'\theta_e')_0}}{bC_TV_0}. \tag{51}$$

Using Eqs. (40) and (44) we can obtain the expression for $\overline{(w'\theta_e')_H}$ without θ_e as

$$\overline{(w'\theta_e')_H}=(F_U-F_H)-\frac{DH}{C_TV_0}\overline{(w'\theta_e')_0} + DH(\theta_{eS}-\theta_{eU}). \tag{52}$$

Finally, it is necessary to provide expressions for the virtual potential temperature flux at the surface, just below cloud base, just above cloud base and at cloud top, respectively. These expressions can be shown by Eq. (26) in the form

$$\overline{(w'\theta_v')_0}=\overline{(w'\theta_e')_0}-\left(\frac{L}{c_p}-\bar{\theta}\delta\right)\overline{w'(q'+m')}, \tag{53}$$

$$\overline{(w'\theta_v')_{h^-}}=\overline{(w'\theta_e')_h}-\left(\frac{L}{c_p}-\bar{\theta}\delta\right)\overline{w'(q'+m')}, \tag{54}$$

$$\overline{(w'\theta_v')_{h^+}}=\left(\frac{1+a\bar{\theta}(1+\delta)}{1+\alpha}\right)\overline{(w'\theta_e')_h}-\bar{\theta}\,\overline{w'(q'+m')}, \tag{55}$$

$$\overline{(w'\theta_v')_H}=\left(\frac{1+a\bar{\theta}(1+\delta)}{1+\alpha}\right)\overline{(w'\theta_e')_H}-\bar{\theta}\,\overline{w'(q'+m')} \tag{56}$$

where

$$\overline{(w'\theta_e')_h}=\left(1-\frac{h}{H}\right)\overline{(w'\theta_e')_o}+\frac{h}{H}\overline{(w'\theta_e')_H}. \tag{57}$$

With the above expressions, GS derivess the closure equation with the use of the weighted average of Lilly's maximum and minimum entrainment in the form

$$\frac{k}{H}\int_0^H \overline{w'\theta_v'}dz+(1-k)\overline{(w'\theta_v')_{\text{minimum}}}=0, \tag{58}$$

where k is a weighting parameter which can take on the values in the range $0 \le k \le 1$. GS assumed that the daily averaged solar radiation is never strong enough to overcome the longwave cooling to produce a net warming effect, the minimum virtual potential temperature flux must always be just below cloud base as seen in Eq. (37). With this in mind, Eq. (58) can be integrated to give

$$\frac{2(1-k)}{k}\overline{(w'\theta_v')_{h^-}} + \overline{(w'\theta_v')_H} + \overline{(w'\theta_v')_{h^+}} + \frac{h}{H}[\overline{(w'\theta_v')_S} + \overline{(w'\theta_v')_{h^-}} - \overline{(w'\theta_v')_H} - \overline{(w'\theta_v')_{h^+}}] = 0. \quad (59)$$

We can solve iteratively until the Eq. (59) is satisfied within some tolerable limits.

4. CTML Model Performance Experiments

4.1 1-D Equilibrium Tests

To evaluate Guinn and Schubert's diagnostic CTML model we perform several one-dimensional sensitivity experiments with the initial conditions as shown in Table 1.

4.1.1 Influence of SST on the CTML

Figure 3 shows the dependence of cloud top and base height as well as the equivalent potential temperature and moisture profiles on SST with the prefixed variables as in Table 1. The result of BR similar to the above SST sensitivity experiment is introduced in the lower-right panel.

The heights of cloud top and base increase gradually with increase in SST. The mixed layer equivalent potential temperature and moisture also increase with the SST increase as shown in the upper-right and lower-left panels, respectively. Both equivalent potential temperature and total water content jumps across the cloud top given in Eq. (43)

Table 1. The initial values used in the 1-D sensitivity test

Variables	Initial values
Initial guess of mixed layer top	1,500 m
Sea-surface temperature	15°C
Large-scale divergence	5 x 10^{-6} s^{-1}
Surface wind speed	10 m/s
Sea-level pressure	1,014 hPa
Vertical profile of equivalent potential temperature (K)	311.5 + 0.00341 x H[1]
Vertical moisture profile (g/kg)	0.001x(5.54 - 0.0012 x H)
Longwave radiation profile (w/m^2)	314.0 - 0.02799 x H

1. H is the cloud top height.

become larger as SST increases due to the heating and moistening of the mixed layer by the enhancement of the surface heat and moisture exchanges across the sea surface. Contrary to the vertical equivalent potential temperature profiles, the vertical moisture profiles show one more step change in the cloud layer. This additional step in the moisture profile represents the fact that some of the water vapor in the mixed layer have been taken away as a result of condensation in the cloud layer. In the proposed CTML model the excessive water vapor over the saturation value with given temperature and pressure values has been converted to the liquid form in the cloud.

As SST increases, thus, the cloud becomes deeper and more moistened, even though the cloud base also increases along with the cloud top. It can be explained as the strong turbulent heat transfer from the sea surface may cause the lifting of condensation level, which is the cloud base height in this proposed model, in spite of the turbulent moisture flux from the sea surface playing a role of lowing condensation level. The behavior of cloud top height dependency on SST's is quite comparable to the results of BR except for the behavior of cloud base which is very sensitive compared to that in BR.

4.1.2 Impacts of large-scale subsidence on the CTML

The large-scale low-level divergence does significantly influence on the formation, maintenance, and dissipation of the marine stratocumulus. Figure 4 shows the dependence of cloud top and base height as well as the vertical equivalent potential temperature and moisture profiles on the large-scale subsidence. The result of BR is also shown in the same way as in Fig. 3. For better comparison the SST value has been chosen as 27°C for this case instead of the prefixed variable in Table 1.

The cloud is very deep when the large-scale low-level divergence is small as shown in Fig. 4. The cloud shrinks rapidly at both top and bottom of the cloud as the large-scale low-level divergence becomes larger. However, the change of cloud base height is less sensitive than the cloud top. Contrary to the SST case the changes of equivalent potential temperature and moisture in the mixed layer are not significant with the change of large-scale divergence. This shallowness of cloud with a large value of divergence

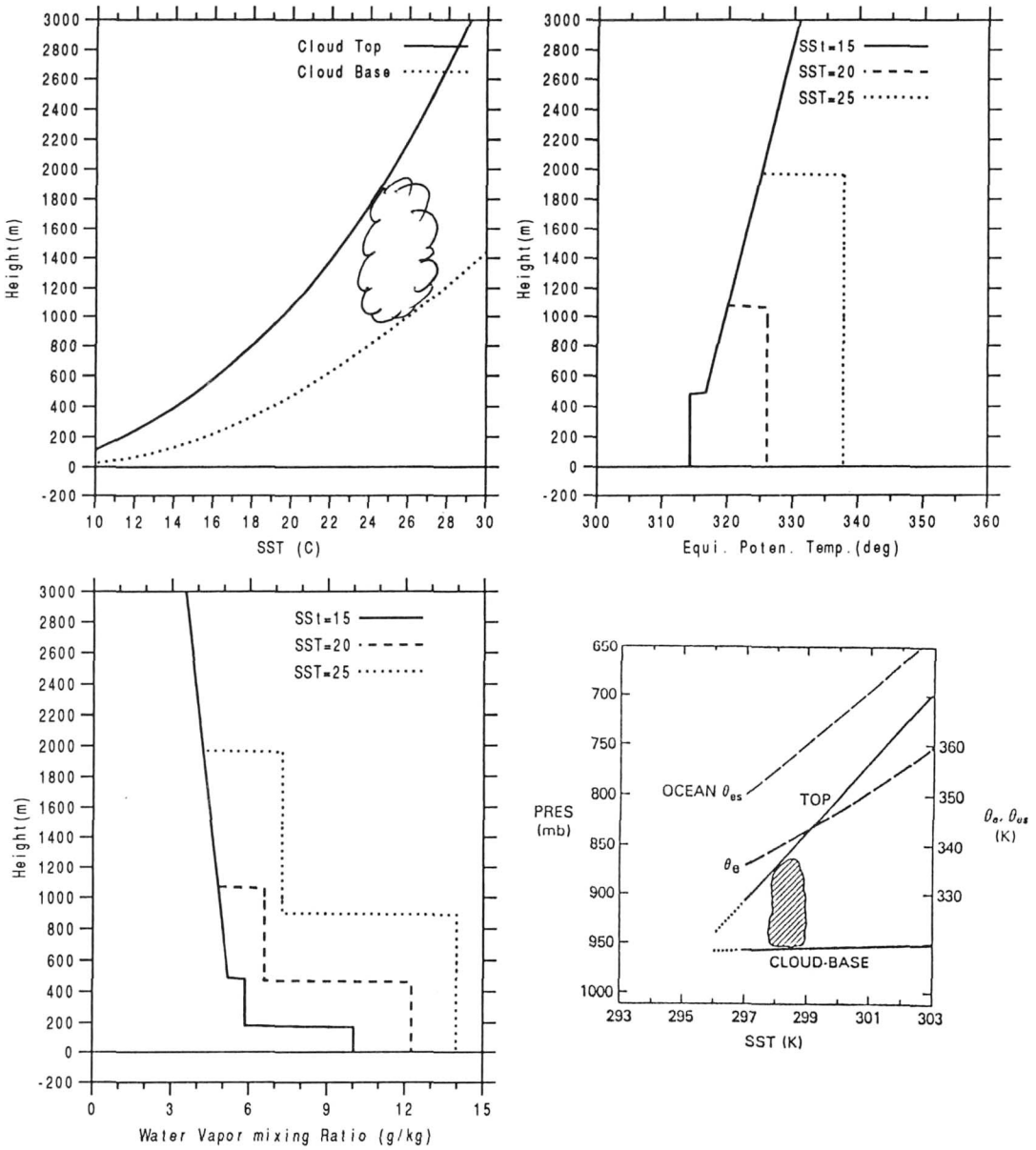

Fig. 3. CTML structure depends on the various SST values: the upper-left panel shows the cloud top (solid) and base (dotted); the upper-right and lower left panel show, respectively, the equivalent potential temperature and moisture profiles for the case of SST = 15 (solid), 20 (dashed), and 25°C (dotted); the lower-right panel shows the similar result of Betts and Ridgway (1989) for the qualitative comparison.

is caused by heating and drying of mixed layer as a result of the subsidence by large-scale divergence at the top of mixed layer. Kloesel (1992) reported that the clearing episodes in the eastern Pacific is partially due to the unusually strong subsidence in this region. This strong subsidence due to the low-level divergence suppresses the formation of marine stratocumulus in the tradewind regions and also causes the dissipation of cloud in this region.

4.1.3 The effect of surface wind speed

The surface wind speed may also play an important

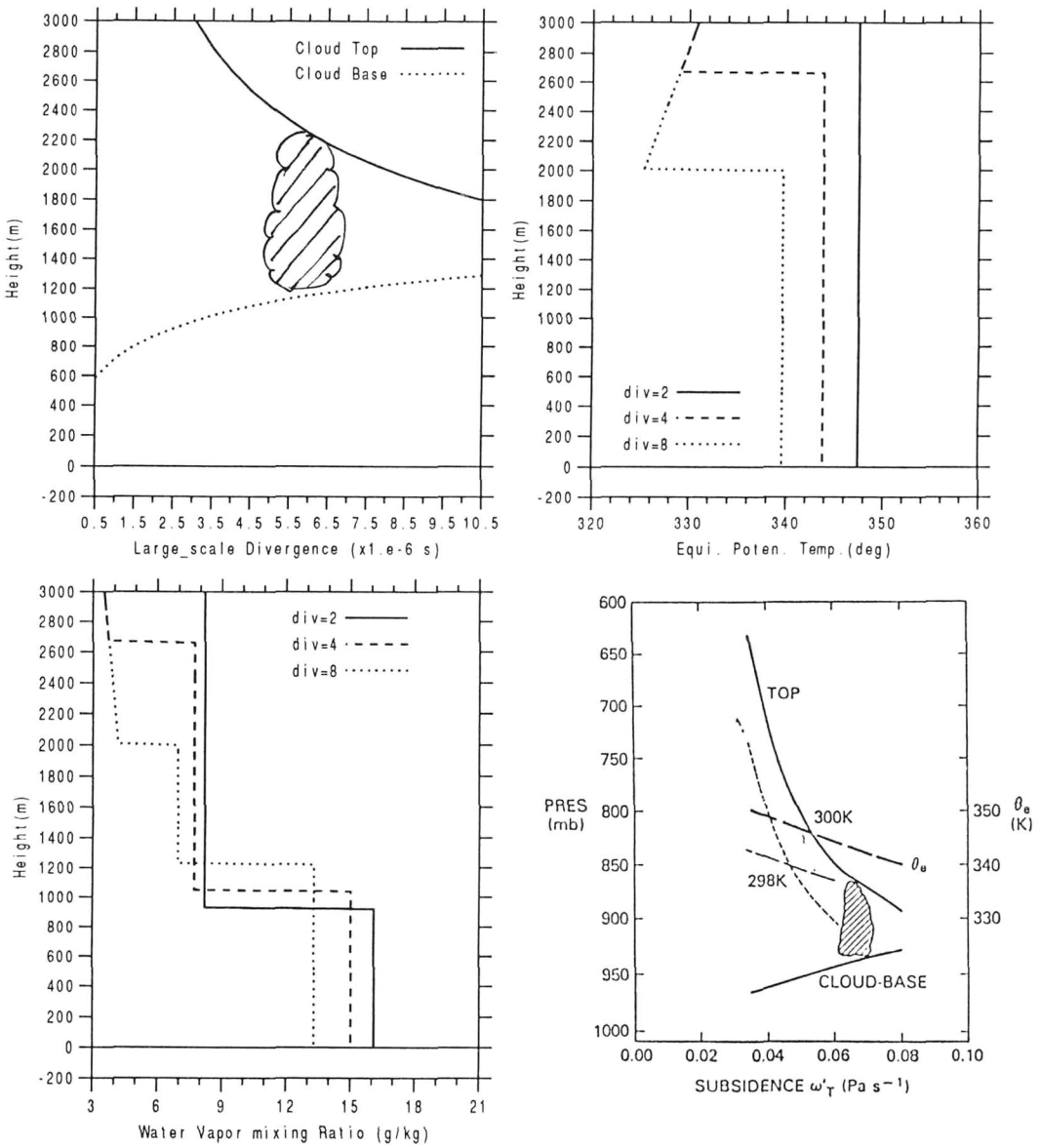

Fig. 4. CTML structure depends on the large-scale low-level divergence: the arrangement of panels is the same as in Fig. 3 except for the case analyses in the upper-right and lower-left panels. Here, the large-scale divergence in the analyzed cases is $2\times$ (solid), $4\times$ (dashed) and $8\times 10^{-6}s^{-1}$ (dotted).

role on developing and maintaining the marine stratocumulus. As in Eqs. (40) and (41), the surface wind can influence on both surface turbulent heat and moisture exchanges. It can be observed in Fig. 5 that the cloud becomes deeper in both directions of the cloud top and bottom as the surface wind speed increases. A similar feature is also observed from BR's work as shown in the lower-right panel of Fig. 5. The cloud can be extended to the high altitude and the cloud base descends as the surface wind speed increases, although the cloud top rising is less sensitive to the wind speed than the cloud base descending. This less sensitiveness of cloud top is somewhat different from Betts and Ridgway's, in

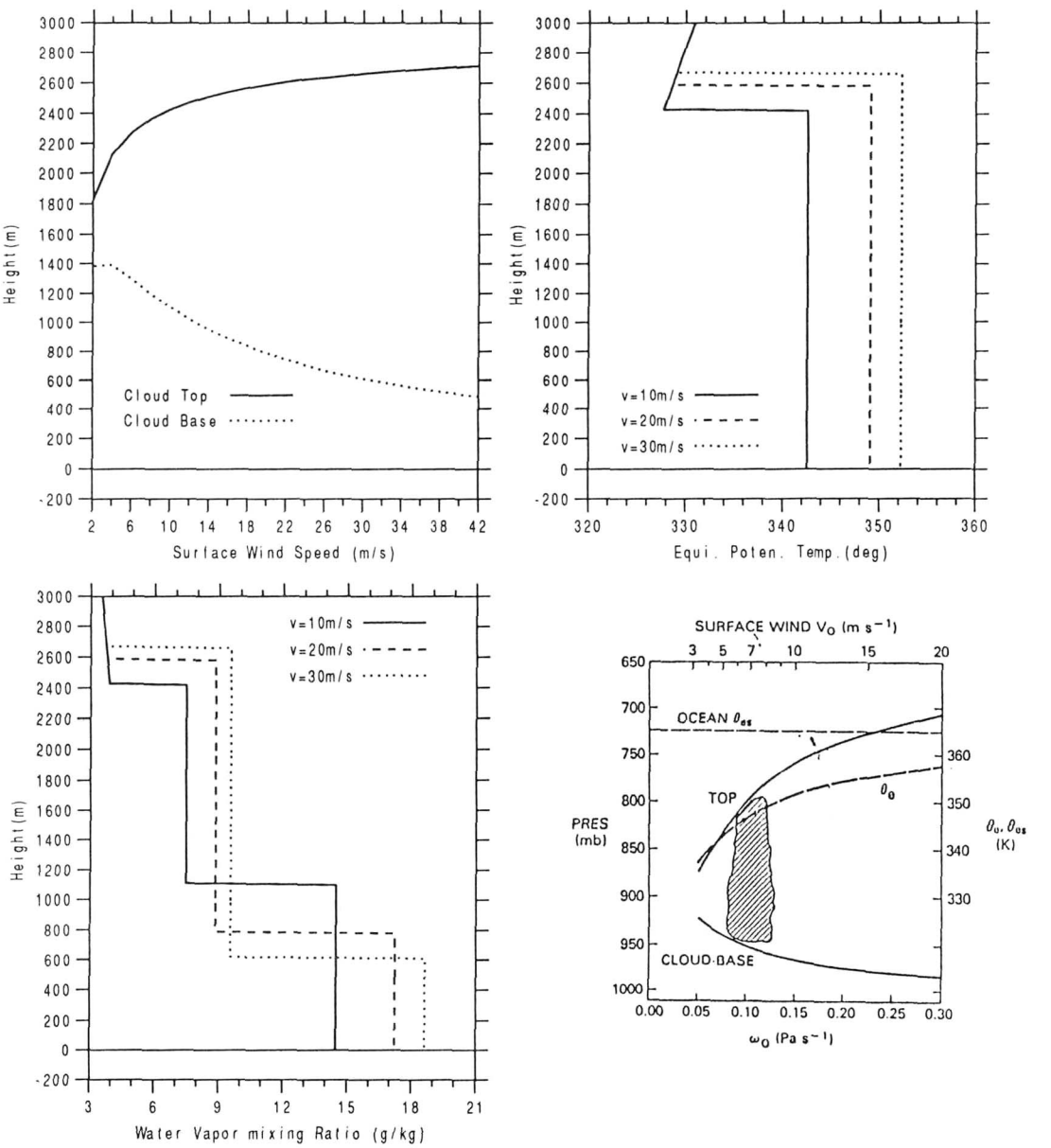

Fig. 5. CTML structure depends on the surface wind speed: the arrangement of panels is the same way as in Fig. 3 except for the case analyses in the upper-right and lower-left panels. Here, the wind speed in the analyzed cases is 10 (solid), 20 (dashed) and 30m/s (dotted).

which the cloud top is more sensitive than the base as shown in the lower-right panel of Fig. 5. As shown in the upper-right and lower-left panel, respectively, the equivalent potential temperature and moisture of the mixed layer also increase along with wind speed, because the turbulent surface sensible heat and moisture exchanges become enhanced as the surface wind speed increases.

4.1.4 Impacts of both SST and large-scale subsidence on the marine stratocumulus

The typical synoptic situations in the eastern Pacific have been introduced by Neiburger *et al.* (1961). Figure 6 shows the mean SST and large-scale

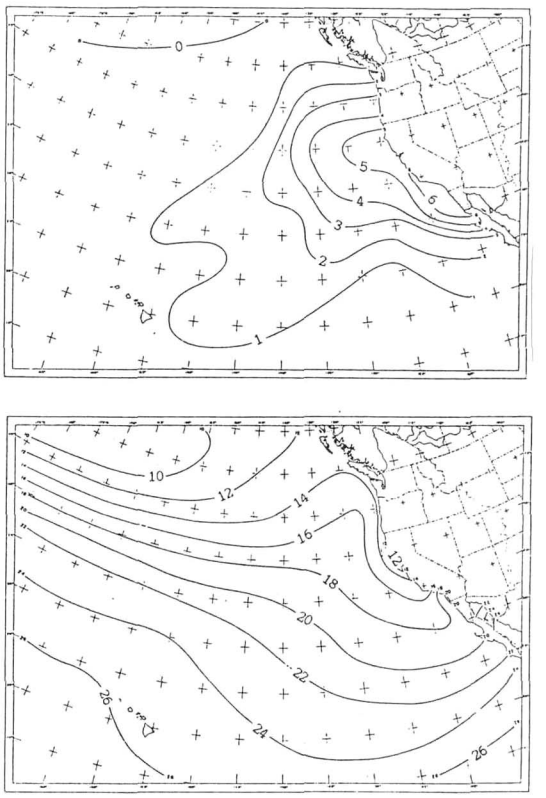

Fig. 6. Low-level divergence (upper) and SST (lower) for July in Neiburger *et al.* (1961). The units are 10-6s-1 and oC for the low-level divergence and SST, respectively.

divergence of the low level in the eastern Pacific during July, respectively, in the upper and lower panel. The isolines of SST in this region are basically distributed along the longitude except near the coastal region of the United States where they are distributed along the coast line and the lowest SST is near the coast. The large-scale low-level divergence becomes larger as close to the coast and shows the maximum at the California coastal region.

To understand the behavior of the marine clouds in this proposed model we performed another sensitivity experiment, in which it was assumed that the SST increases from 12°C to 30°C as it moves to the south and the low-level large-scale divergence also varies from $1 \times 10^{-6}s^{-1}$ to $1 \times 10^{-5}s^{-1}$ as it moves from the mid-Pacific ocean to the coast. Figure 7 shows the distribution of cloud top and base height, respectively, in the upper and lower panel. It can be easily observed that the clouds by this proposed model form in the

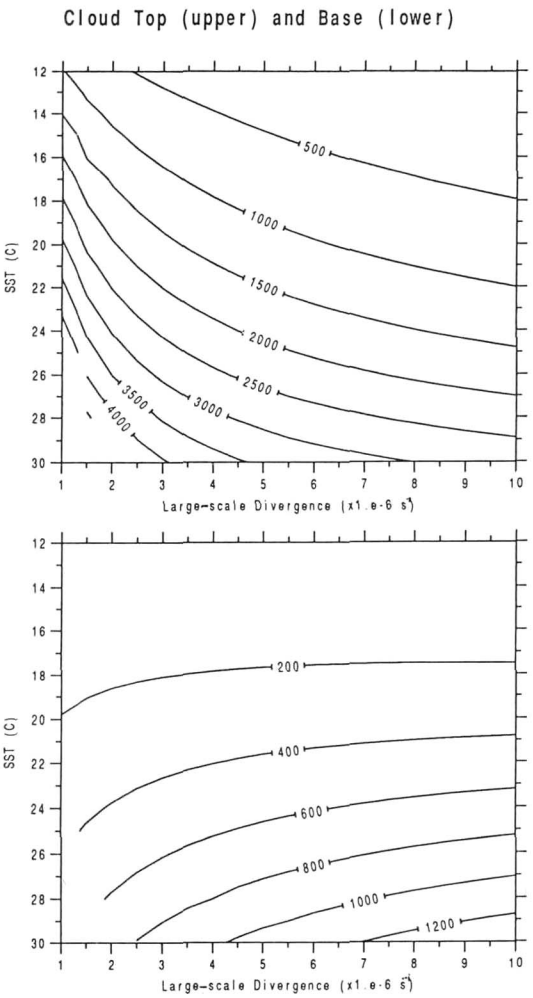

Fig. 7. The height of cloud top (upper) and base (lower) depend on the SST and the large-scale subsidence.

height range of 100 m to 4,000 m in this subtropical region except the region where the SST is larger than 28°C. It is hard to justify the application of this CTML model instead of the deep cumulus parameterization over the ocean where the SST is larger than 28°C.

The cloud becomes deeper as it goes to the south and shallower as it moves to the coast as shown in Fig. 7, in which the increasing SST corresponds to lowering latitude and the increasing large-scale divergence as moving toward the U.S. Coast. As a result of relatively weak surface heat and moisture supply from the ocean we may expect a fog or low and shallow clouds in the northern U.S. coastal region. Both the cloud top and base increase as it moves to the

warm oceanic area due to a strong heat and moisture supply from the warm ocean. As shown in the upper panel of Fig. 7 the cloud top height exhibits a strong sensitivity to both SST and large-scale divergence. The cloud base height is not much sensitive to the large-scale low-level divergence, however. The clouds near the ITCZ (Intertropical Convergence Zone) may form in the vertical range of about 1,000 m to 3,500 m under the conditions shown in Fig. 6. Beyond the SST range of 28°C or higher it may not be a good idea to use the proposed scheme. This region may be characterized to tropics so that there is a large-scale low-level divergence hardly. The deep convection parameterization is more adequate to represent the clouds.

4.2 GCM Experiments

We introduced the Guinn and Schubert model (1989) to the YONU GCM, which has been developed from the dynamical structure of the MRI GCM (Tokioka *et al.*, 1985) and the physical parameterizations of the UILL GCM (Oh, 1989). Following additional modifications were made on the GS model for its application to YONU GCM: the tolerance value of iteration to find a suitable solution of Eq. (59) is eased to 10m instead of 0.01m with the consideration of the relatively coarse vertical resolution of the GCM and the maximum number of iteration is limited to 10 rather than 50 for the economic computation. If the cloud, which might be generated by the earlier large-scale condensation or convection, exists in the lowest four layers, we ignore this type of cloud process to avoid a complicated situation. The downward shortwave and longwave radiation at the top of cloud is interpolated linearly with height using those values at top and bottom of the layer in which the cloud is located. We also assume that 10% of the incoming solar radiation at the top of cloud is absorbed in the mixed layer instead of a constant value (= 22.3 Wm^{-2}) used in Lilly (1968) and GS. The values of equivalent potential temperatures and moisture at the cloud top are interpolated linearly in height by a similar manner used for the radiation variables.

The radiation scheme employed in the YONU GCM requires the values of cloud liquid/ice water amounts and cloud types to calculate the cloud optical properties. In the GCM the cloud liquid/ice water amount of stratiform and cumuloform cloud is treated as one of prognostic variables. Then, the cloud optical properties such as optical depth, single scattering albedo and asymmetric factor are calculated from the cloud liquid/ice water amount by taking account of cloud types and solar zenith angles (Oh *et al.*, 1994). In coupling of this diagnostic CTML model with YONU GCM, however, the absence of the cloud liquid water information has been overcome by using the preset the cloud liquid water content based on Fairall *et al.* (1990).

The YONU GCM has been integrated only for June and July in the case of with CTML model (Test Run)

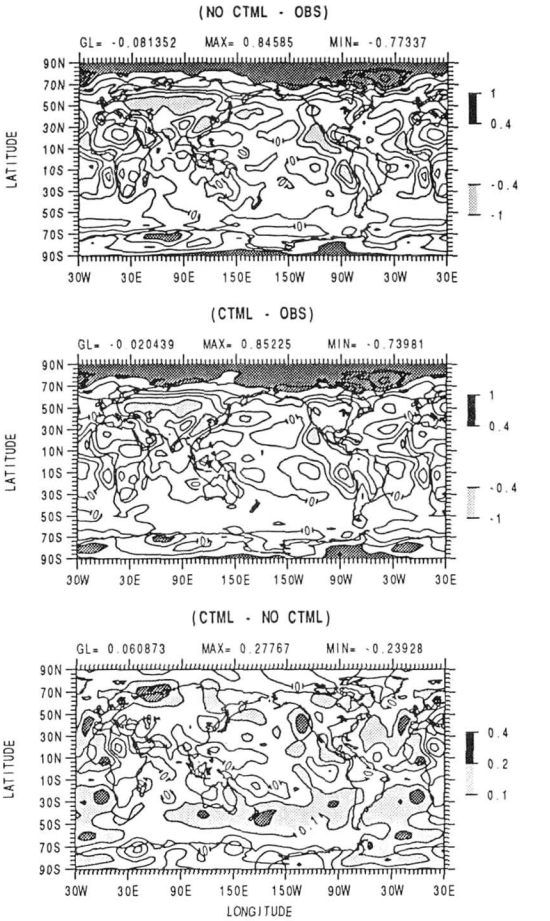

Fig. 8. The total cloudiness difference from the ISCCP data during July without (upper) and with the CTML (middle) together with their difference between two cases. The region where the clouds were increased due to the CTML is shaded.

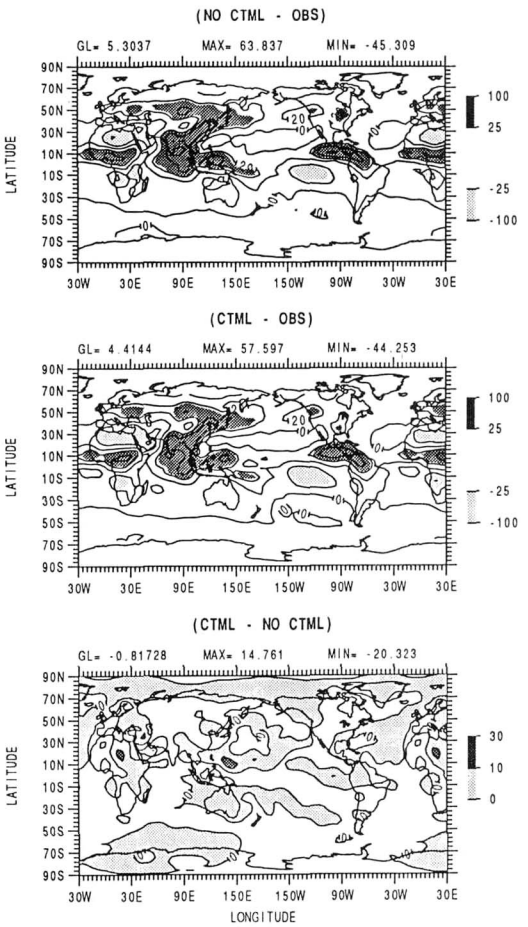

Fig. 9. Same as in Fig. 8 except for OLR.

and without CTML model (Control Run). The reason of this relatively short integration is mainly due to the fact that the results obtained in a full model, such as GCM, is often difficult to provide conclusive evidence about the parameterization of a single process like CTML model proposed in this study.

Figures 8 and 9 show, respectively, the differences of July cloudiness and outgoing longwave radiation (OLR) of the control run (upper panel) and the test run (middle panel) from the data of International Satellite Cloud Climate Project (ISCCP, Rossow, and Schiffer, 1991) and Earth Radiation Budget Experiment (ERBE, Kyle *et al.*, 1990), together with their differences between above two cases. The region where the test run gives less clouds is shaded and the contours are in every one-tenth of total cloudiness difference. Without this CTML model the underestimation of as large as 40% are observed at the west coastal regions of America and Africa as shown in the upper panel. The simulation of clouds in the subtropical regions, particularly in the southern hemisphere, has been significantly improved with the CTML model, although the cloudiness over the west coastal regions of continents are still underestimated as shown in the middle panel. The impact of CTML model on the simulation of fractional cloudiness can be easily seen in the lower panel. The region where the clouds increase due to CTML model is shaded. As shown in the lower panel the cloudiness increases in the west coastal region where the cloud underestimation is significant without the CTML scheme. However, the OLR in the corresponding area is not much different whether the CTML is included or not. This little change of OLR in the face of increasing fractional cloudiness in the subtropical regions is mainly due to the fact that the clouds formed by CTML model are the low-level clouds so that the cloud-top temperature may not be too different from SST.

5. Summary and Conclusion

Before coupling the diagnostic CTML model with GCM we perform several one-dimensional sensitivity experiments to evaluate the performance of this proposed CTML model. The results can be summarized as:

1) As SST increases, the cloud becomes deeper and more moistened, although the cloud base also increases along with the cloud top. The strong turbulent heat fluxes from the sea surface may cause the lifting of the mixed layer and the condensation level in spite of the turbulent moisture flux which may play a role for lowering this condensation level.

2) The cloud can be very deep with a small large-scale low-level divergence, however, the large-scale low-level divergence may shrink the cloud thickness vertically in both directions. The equivalent potential temperature and moisture of the mixed layer are not much sensitive because this large-scale divergence mainly affects on the cloud top height by modifying the heat and moisture fluxes at the top of mixed layer.

3) The cloud becomes deeper by lowering the bottom and elevating the top and the equivalent

potential temperature and moisture in the mixed layer also increase as the wind speed increases due to the enhanced surface sensible heat and moisture exchanges.

4) Under the typical synoptic situations in the eastern Pacific the proposed CTML model predicts the existance of the marine clouds may exist in the vertical range of 100 m to 4,000 m. The cloud becomes deeper as it goes to south and shallower as it moves to U.S. coast. Fog or low and shallow clouds have been expected in the northern part where SST is colder than 15°C. The deep convection parameterization may be more adequate to represent the tall clouds near the ITCZ.

From a series of two months GCM integration experiments we observe the proposed CTML model improves the underestimated subtropical marine clouds without this CTML model. We may conclude that the proposed diagnostic CTML model has a capability to improve notably the marine stratocumulus at the region of the large-scale mass divergence and the oceanic cool waters in the trade-wind zone.

In spite of the above successes on the implementation of the mixed layer cloud scheme in the GCM there are still many tasks to overcome as summarized by Browning (1994). For example, the YONU GCM employs a prognostic cloud scheme, in which the cloud liquid/ ice water and the partial cloudiness are calculated prognostically and semi-prognostically, respectively. Therefore, more efforts are required to enhance the treatment of boundary-layer clouds in the GCM to be fully comparable to the parameterization of the other cloud types in the YONU GCM. Meanwhile, recent observational studies by Peterson *et al.* (1992) and Klein and Hartmann (1993) showed a strong correlation between SST and cloud cover or cloud albedo. This kind of observational studies can be another strong motivation to study the precise representation of marine stratocumulus in the GCMs.

Acknowledgments

We thank I. U. Chung for his assistance to perform the GCM sensitivity experiments. Also, we are very thankful to anonymous reviews for constructive comments and suggestions. This research was supported by the Ministry of Education under Grant for the university laboratory.

Appendix A

The Clausius-Clapeyron equation is given as

$$de_s = \frac{\delta L}{RT^2} e_s dT. \tag{A.1}$$

Here, from the definition of the q^* in terms of e_s and p

$$de_s = \frac{p}{\delta} dq^* + \frac{q^*}{\delta} dp, \tag{A.2}$$

and from the poissons' equation

$$\frac{dT}{T} = \frac{d\theta}{\theta} + \frac{R}{c_p}\frac{dp}{p}. \tag{A.3}$$

Substituting Eqs. (A.2) and (A.3) into Eq. (A.1) we obtain

$$\frac{p}{\delta} dq^* + \frac{q^*}{\delta} dp = \frac{\varepsilon L}{RT}\left(\frac{p}{\delta} q^*\right)\left(\frac{d\theta}{\theta} + \frac{R}{c_p}\frac{dp}{p}\right) \tag{A.4}$$

or

$$dq^* = \frac{\varepsilon L}{RT} q^* \frac{1}{\theta} d\theta - \frac{g}{RT} q^* \left(\frac{\varepsilon L}{RT} - 1\right) dz. \tag{A.5}$$

References

Albrecht, B.A., A. Betts, W.H. Schubert, and S.K. Cox, 1979: A model of the thermodynamic structure of the trade wind boundary layer: Part I. Theoretical formulation and sensitivity tests. *J. Atmos. Sci.*, 36, 73-89.

————, D.A. Randall, and S. Nicholls, 1988: Observations of marine stratocumulus clouds during FIRE. *Bull. Amer. Meteor. Soc.*, 69, 618-626.

————, M.B. Baker, C.S. Bretherton, J.A. Coakley, C.W. Fairall, B.J. Huebert, M.D. King, D.S. McDougal, D.A. Randall, W.H. Schubert, J.B. Sinder, B.A. Wielicki, and D.P. Wylie, 1990: *FIRE Phase II: ASTEX Implementation plan.* FIRE Project Office, NASA Langley Research Center, Hampton, VA, 137pp.

Ball, F.K., 1960: Control of inversion height by surface heating. *Quart. J. R. Meteor. Soc.*, 86, 483-494.

Betts, A.K., 1973: Non-precipitating cumulus convection and

its parameterization. *Quart. J. Roy. Meteor. Soc.*, 99, 178-196.

————, and W. Ridgway, 1989: Climatic equilibrium of the atmospheric convective boundary layer over a tropical ocean. *J. Atmos. Sci.*, 46, 2621-2641.

————, and R. Bores, 1990: A cloudiness transition in a marine boundary layer. *J. Atmos. Sci.*, 47, 1480-1497.

Browning, K.A., 1994: Survey of perceived priority issues in the parameterizations of cloud-related processes in GCMs. *Quart. J. Roy. Meteor. Soc.*, 120, 483-487.

Charlson, R.J., J.E. Lovelock, M.O. Andreae, and S.G. Warren, 1987: Oceanic phytoplankton, atmospheric sulfur, cloud albedo and climate. *Nature*, 326, 655-661.

Chen, C., and W.R. Cotton, 1987: The physics of the marine stratocumulus-capped mixed layer. *J. Atmos. Sci.*, 44, 2940-2950.

Cox, S.K., D. McDougal, D. Randall, and R. Shiffer, 1987: FIRE - the First ISCCP regional Experiment. *Bull. Amer. Meteor. Soc.*, 68, 114-118.

Guinn, T.A., and W.H. Schubert, 1989: Stratus: An interactive mixed layer model for personal computers (Version 1.0). Department of Atmospheric Sciences, Colorado State University, Fort Collins, CO.

Fairall, C.W., and J.E. Hare, 1990: An eight-month sample of marine stratocumulus cloud fraction, albedo, and integrated liquid water. *J. Climat.*, 3, 847-864.

Kloesel, K.A., 1992: Marine stratocumulus cloud clearing episodes observed during FIRE. *Mon. Wea. Rev.*, 120, 565-578.

Kyle, H.L., A. Mecherikunnel, P.E. Ardanuy, L. Penn, B. Groveman, G.G. Campbell and T.H. Vonder Harr, 1990: A comparison of two major earth radiation budget data sets. *J. Geophys. Res.*, 95, 9951-9970.

Lilly, D.K., 1968: Models of cloud-topped mixed layers under a strong inversion. *Quart. J.Roy. Meteor. Soc.*, 94, 292-309.

Neiburger, M., D.S. Johnson, and C.W. Chien, 1961: Studies of the structure of the atmosphere over the Eastern Pacific Ocean in summer, I: The inversion over the Eastern North Pacific Ocean. *Univ. Calif. Publ. Meteor.* 1, No. 1.

Oh, J.-H., 1989: Physically-based general circulation model parameterization of clouds and their radiative interaction. Ph.D. dissertation, Department of Atmospheric Sciences, Oregon State University, Corvallis, OR, 315 pp.

————, J.-H. Jung, and J.-W. Kim, 1994: Radiative transfer model for climate studies: 1. Solar radiation parameterization and validation. *J. Korean Meteor. Soc.*, 30, 315-333..

Oreopoulos, L., and R. Davies, 1993: Statistical dependence of albedo and cloud cover on sea surface temperature for two tropical marine stratocumulus regions. *J. Climate*, 6, 2434-2447.

Peterson, T.C., T.P. Barnett, E. Rockener, and T.H. Vonder Harr, 1992: An analysis of the relationship between cloud anomalies and sea surface temperature anomalies in a global circulation model. *J. Geophys. Res.*, 97, 20, 497-20,506.

Randall, D.A., J.A.Coakley Jr., C.W. Fairall, R.A. Kropfil, and D.H. Lenshow, 1984: Outlook for research on subtropical marine stratiform clouds. *Bull. Amer. Meteor. Soc.*, 65, 1290-1301.

————, Q. Shao, and C.-H. Moeng, 1992: A second-order bulk boundary layer model. *J. Atmos. Sci.*, 49, 1903-1923.

Rogers, D.P., and D. Koracin, 1992: Radiative transfer and turbulence in the cloud-topped marine atmospheric boundary layer. *J. Atmos. Sci.*, 49, 1473-1486.

————, J.A. Businger, and H. Charnock, 1985: A numerical investigation of the JASIN atmospheric boundary layer. *Bound.-Layer Meteor.*, 37, 373-399.

Rossow, W.B., and R.A. Schiffer, 1991: ISCCP cloud data products. *Bull. Amer. Meteor. Soc.*, 72, 2-20.

Schubert, W.H., J.S. Wakefield, E.J. Steiner, S.K. Cox, 1979: Marine stratocumulus convection. Part 1: Governing equations and horizontally homogeneous solutions. *J. Appl. Meteorol.*, 36, 1286-1307.

Tokioka, T, A. Kitoch, I. Yagai and K. Yamazaki, 1985: A simulation of the tropospheric general circulation with the MRI atmospheric general circulation model. Part I: The January performance. *J. Met. Soc. Japan*, 63, 749-778.

Wang, S., 1993: Modeling marine boundary-layer clouds with a two-layer model: A one-dimensional simulation. *J. Atmos. Sci.*, 50, 4001-4021.